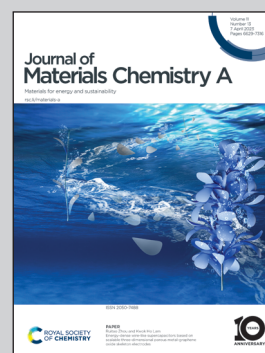


A study on the extraction of citrated cellulose nanocrystals from cotton textiles was conducted at Stockholm University, led by Professor Aji Mathew in collaboration with RISE—Research Institutes of Sweden and VTT—Technical Research Centre of Finland.

Citrated cellulose nanocrystals from post-consumer cotton textiles

The main steps for the extraction of citrated cellulose nanocrystals (CitCNCs) from post-consumer cotton textiles are shown. An esterification with citric acid followed by mechanical fibrillation results in CitCNCs with high yield and high surface charge attributed to the carboxylic groups covalently attached *via* mono and di-ester linkages.








As featured in:



See Aji P. Mathew *et al.*,
J. Mater. Chem. A, 2023, **11**, 6854.

Cite this: *J. Mater. Chem. A*, 2023, **11**, 6854

Citrated cellulose nanocrystals from post-consumer cotton textiles†

Maria-Ximena Ruiz-Caldas, ^a Varvara Apostolopoulou-Kalkavoura, ^a Anna-Karin Hellström, ^b Jutta Hildenbrand, ^b Mikael Larsson, ^b Aleksander Jaworski, ^a Joseph S. M. Samec, ^c Panu Lahtinen, ^d Tekla Tammelin ^d and Aji P. Mathew ^{*a}

We propose a new method for the extraction of cellulose nanocrystals (CNCs) from post-consumer cotton textiles through surface functionalization followed by mechanical treatment. Cotton-based textiles were esterified using an 85 wt% solution of citric acid at 100 °C, then further fibrillated in a microfluidizer. The final product, citrated cellulose nanocrystals (CitCNCs), was a dispersion of needle-like nanoparticles with high crystallinity. Up to 78 wt% of the cotton fabric was converted to CitCNCs that exhibited higher yields and a higher surface group content than CNCs extracted through H₂SO₄ hydrolysis, although CitCNCs showed a broader size distribution and decreased thermal stability. Experimental data supported by DFT calculations showed that the carboxyl groups on the CitCNC surface are bonded to cellulose by mono or diester linkages. An early-stage life cycle assessment (LCA) was performed to evaluate the environmental impact of using discarded textiles as a source of cellulose and analyze the environmental performance of the production of CitCNCs. Our work showed a significant reduction in the environmental burden of CNC extraction using post-consumer cotton instead of wood pulp, making clothing a good feedstock. The environmental impact of CitCNC production was mainly dominated by citric acid. As a proof of concept, around 58 wt% of the citric acid was recovered through evaporation and subsequent crystallization, which could reduce climate impact by 40%. With this work, we introduce a catalyst-free route to valorize textiles with the extraction of CitCNCs and how conducting LCA in laboratory-scale processes might guide future development and optimization.

Received 5th December 2022
Accepted 15th February 2023

DOI: 10.1039/d2ta09456h

rsc.li/materials-a

Introduction

Clothing is considered a basic need for humans,¹ but the expansion of fast fashion, the drop in market prices, and the increased efficiency of textile production and delivery have increased the consumption of clothing worldwide.^{2,3} According to recent statistics, an EU national consumes around 26 kg of textiles and discards around 11 kg every year.³ The clothing industry is based on a linear model on which the largest share of post-consumer textiles is incinerated or landfilled,^{3,4} while the garments collected for recycling are mainly diverted to other applications (e.g., insulating materials, cleaning cloths, etc.), and only 1% of raw materials are recycled back for producing new clothing.⁴ With growing environmental awareness and

considering the societal and economic impacts of textile waste, the need to find new routes for textile recycling becomes essential.

Textile waste is composed of both natural and synthetic fibers. Cotton is the major natural fiber used in the clothing industry and represented approximately 24% of global fiber production in 2020.⁵ The production of cotton has heavy environmental impacts mainly due to the huge amounts of water required, land occupation, and use of pesticides for its cultivation.⁶ As cotton cultivation severely contributes to water scarcity and pollution, there is a great need to look for alternatives that extend the life cycle of cotton, for example, transforming post-consumer cotton into high-quality materials.

Cellulose nanomaterials (CNMs) are isolated from cellulose sources following mechanical and chemical routes. In recent decades, CNMs have generated great interest as reinforcement agents and building blocks for functional materials due to their renewability, biocompatibility, tunable surface chemistry, high specific surface area, low density, low thermal conductivity, and good mechanical properties.^{7,8} CNMs can be extracted from a wide range of sources, such as wood, cotton, ramie, sisal, flax,

^aDepartment of Materials and Environmental Chemistry, Stockholm University, SE-10691 Stockholm, Sweden. E-mail: aji.mathew@mmk.su.se^bRISE—Research Institutes of Sweden, Mölndal, SE-43153, Sweden^cDepartment of Organic Chemistry, Stockholm University, SE-10691 Stockholm, Sweden^dVTT Technical Research Centre of Finland, Tietotie 4E, FI-02044 VTT, Finland† Electronic supplementary information (ESI) available. See DOI: <https://doi.org/10.1039/d2ta09456h>

tunicate, and algae,⁷ and their properties vary depending on the cellulose source they are extracted from ref. 9 and 10.

One of the challenges associated with the widespread use of CNMs is their sustainability.⁹ There have been continuing efforts to produce CNMs more sustainably, including the extraction from waste biomaterials such as agricultural residues, industrial residues, and side streams. This might be a promising solution to valorize cotton-sourced materials through safe and sustainable routes. Besides, extracting nanocellulose from textiles can diminish most of the defects on the fibers, which are mainly caused by everyday use and laundering, while producing cellulose-based nano “building blocks”. These building blocks show great potential for use in diverse areas such as composites and energy.^{11,12}

Although wood is the main source of cellulose for the extraction of CNMs,¹³ multiple steps are necessary for isolating pure cellulose from wood¹⁴ since wood contains between 40–50% cellulose.¹⁵ Cotton fibers, on the other hand, are the purest form of cellulose,¹⁶ and possess a high degree of polymerization and crystallinity¹⁶ among plant-based cellulose sources. Therefore, discarded cotton textiles can be seen as a valuable raw material and source of CNMs.

Cellulose nanocrystals (CNCs) are rod-like nanomaterials with high crystallinity commonly extracted through acid hydrolysis.¹⁰ In our previous work, we extracted CNCs from post-consumer cotton and blended fabrics through sulfuric acid hydrolysis.¹⁷ Our results showed that while residual dyes remained attached to the nanocrystals, their properties were equivalent to CNCs extracted from virgin cotton.¹⁷ There have also been a few other studies attempting to recycle cotton textiles by following different disintegration routes such as hydrolysis,^{18–20} and oxidation,^{20,21} or through some mechanical treatment (*i.e.*, shredding) to use the fibers as reinforcement material.²² New routes for waste valorization could induce subsequently environmental impacts and costs, so it is important to also evaluate the feasibility of these routes from an environmental sustainability point of view. Besides, performing these evaluations on the lab scale will help to identify the critical steps in the earlier stages and guide research efforts to improve the sustainability performance of a new route.

Life-cycle assessment (LCA)²³ is a widely used tool for environmental analysis. LCA is a standardized method used to evaluate the impact associated with all life cycle stages of a product or material from the extraction of raw materials (cradle) to end-of-life (grave) and disposal, including potential recycling routes, and considering the resources used in all stages such as chemicals, materials, water, and energy. Despite the high uncertainty of laboratory data, implementing LCA studies in the early stages can assist in identifying hotspots²⁴ which can facilitate future scale-up. Multiple studies have been done assessing the environmental impact of the production and/or applications of cellulose nanofibrils^{25–27} and CNCs.^{28–30} For example, Bondancia and colleagues²⁹ assessed the environmental performance of the extraction of CNCs from sugar cane bagasse through organic and/or inorganic acid hydrolysis and showed the environmental burden of using citric acid as hydrolysis media.

In this work, we present a route for the valorization of post-consumer cotton textiles through the extraction of CNCs by functionalization with citric acid and subsequent fibrillation. Citric acid is a tricarboxylic acid commercially produced by fermentation that can react with cellulose to produce cellulose citrate.^{31,32} Previous studies have shown that it is possible to extract CNCs from multiple sources using organic acids^{33,34} including citric acid,^{35–40} but to the best of our knowledge, this is the first report on real post-consumer cotton-based fabrics, and of CNC extraction in high-yield through the combination of chemical and mechanical treatments. By implementing an LCA study based on laboratory-scale data, we evaluated the environmental impact of using cotton textiles as the source of cellulose over wood pulp, and the environmental burden of each process stage of our route and identified its environmental hotspots. The novelty presented in the current work is not only the possibility of efficiently valorizing old cotton garments but also identifying the bottlenecks of new lab-scale routes in terms of sustainability.

Experimental section

Materials

Wargön Innovation kindly provided post-consumer cotton fabrics that were sourced and sorted from other post-consumer fabrics through clothing tags and visual inspection and cleaned of any seams, prints, or other details before being shipped. No chemical treatments were performed on the fabrics and were used as received. For more detailed information about the sorting of the cotton fabrics made by Wargön, refer to “Life Cycle Assessment” in the Experimental section.

The following chemicals were used as received: standardized sodium hydroxide (NaOH, 0.1 M Fisher Chemical™), sodium hydroxide pellets (>98% Honeywell Fluka™), citric acid anhydrous (99 wt% Thermo Scientific™), hydrochloric acid (37 wt% AnalaR® Normapur®), copper(II) sulfate pentahydrate (99+% Thermo Scientific™), and murexide (ACS reagent Sigma-Aldrich). Deionized (DI) water was used throughout the study.

Esterification and partial hydrolysis of cotton

Textile garments were cut into small (<1 cm²) pieces and placed into a round-bottom flask containing an aqueous solution of citric acid at a concentration of 85 wt%. The ratio of textile to pure citric acid was 1 : 20 (g g⁻¹). The flask was immersed in an oil bath and heated to 100 °C under stirring at 300 rpm using an overhead mechanical stirrer. After ensuring that the citric acid was fully dissolved, the reaction took place for seven hours before it was quenched by a five-fold dilution with DI water. The quenched mixture was vacuum filtered onto a polyethersulfone (PES) membrane (pore size 5 μm) to separate the citric acid solution from the solid fraction that contained carboxylated cotton fibers and residual acid. The first litter of the effluent after quenching was collected, and the citric acid was recovered by evaporation and crystallization. DI water was gently added to the filter cake to rinse out the remaining citric acid from the solid. The carboxylated cotton cake was washed until the conductivity of the filtrate was below 5 μS cm⁻¹.



Mechanical fibrillation

The filter cake of esterified cotton fabrics was diluted with DI water to a concentration of approx. 2 wt% and dispersed with an Ultra-Turrax® rotor-stator mixer (IKA) at 10 000 rpm for 10 min. The obtained dispersion was neutralized by adding drops of NaOH (aq, 1 M) until reaching a pH of 7.0, then diluted to 1.0 wt% and fibrillated using a high-pressure microfluidizer (M-110EH, Microfluidics). Five passes through 400- and 200 µm-wide chambers connected in series were performed at 1000 bar and were followed by five passes through 200- and 100 µm-wide chambers at 1700 bar. After mechanical fibrillation, the resulting dispersion was centrifuged at 10000g for 10 min and vacuum filtered through a glass microfiber filter (Ahlstrom-Munksjö MGF grade, particle retention 0.7 µm) to remove traces of non-fibrillated cotton. The final product was a colloidal dispersion of CNCs with surface carboxylic groups in sodium form (–COONa). The mass recovery yield was calculated as the mass of CNCs per mass of cotton. A fraction of the CNC dispersion was freeze-dried for further characterization.

Characterization

Atomic force microscopy (AFM). The morphology of the CNCs was recorded using Multimode-8 AFM (Bruker, USA). The imaging was conducted in peak-force tapping mode, using the manufacturer's ScanAsyst™ automatic optimization algorithm. The samples were prepared by adding a few drops of 0.001 wt% CNC dispersion onto the surface of a freshly cleaved mica and left drying at room temperature. Image analysis was carried out using the software Gwyddion 2.60 measuring at least 200 nanoparticles of each type of CNCs (SCNCs and CitCNCs).

Zeta potential. Zetasizer Nano ZS (Malvern Instruments Ltd., Malvern, UK) was used to measure the zeta potential of CNC dispersions of 0.1 wt%. Solutions of HCl (10 mM) or NaOH (10 mM) were used to set the pH of the dispersions at the desired value. The measurements were conducted in a background electrolyte solution containing 1 mM NaCl over a pH range of 2–12 at 25 °C. A stock solution of NaCl 1 M was used to tune the ionic strength without significantly changing the concentration. Each sample was measured a total of five times, with each measurement composed of at least 10 cycles.

X-ray diffraction. X-ray powder diffraction measurements were carried out using a Panalytical X'Pert Pro diffractometer (Cu Kα1,2, λ₁ = 1.540598 Å, λ₂ = 1.544426 Å) in Bragg–Brentano geometry operated at 45 kV and 40 mA. For CNCs, the measurements were performed over pellets made of freeze-dried CNCs prepared by molding ~200 mg of freeze-dried CNCs into a pellet using a hydraulic KBr press, while cotton pieces were measured without any sample preparation. Continuous scans with 2θ ranging from 5° to 60° were collected with a step size of 0.01° and a scan speed of about 0.1° s^{–1}. A beam knife slit was positioned above the pellet. During acquisition, the sample rotated with a revolution time of 2 s. The diffraction peaks were fitted with Voigt peak functions, assuming a linear background, while the amorphous region was fitted as a broad peak centered at 2θ = 20.6° (ref. 41). The

deconvolution of each diffractogram was carried out using Fitlyk peak-fitting software.⁴²

Thermal analysis. Thermogravimetric (TGA) and derivative thermogravimetric (DTG) analyses were carried out on a TA Instruments Discovery thermogravimetric analyzer. Around 10 mg of either freeze-dried CNCs or cotton textiles were placed in a platinum pan and heated at a rate of 10 °C min^{–1} from ambient temperature to 600 °C under nitrogen atmosphere at a gas flow rate of 100 mL min^{–1}.

Moisture uptake. Around 120 mg of freeze-dried CNCs were placed inside a desiccator with silica gel and weighed after 24 h (*W*_{dry}), then placed in a desiccator with a saturated solution of potassium chloride to reach a humidity of around 84%. The samples were reweighed after 24 h (*W*_{wet}) and returned to the desiccator. The moisture uptake was calculated using the equation below and performed on five samples per CNC type.

$$\text{Moisture uptake}(t: \text{days } (\%)) = \frac{W_{\text{wet}} - W_{\text{dry}}}{W_{\text{dry}}}$$

Carboxyl and citrate group content. The carboxyl content was determined through conductometric titrations using a conductivity meter (SevenExcellence, Mettler Toledo). Around 200 mg of sample were diluted to a concentration of 0.2 wt% with DI water and some drops of HCl 0.5 M were added to decrease the pH below 2.5. The samples were titrated with aliquots of standardized NaOH 0.1 M (Titripur®). The conductivity was measured throughout the titration leaving 30 s for stabilization after the addition of NaOH. The inflection point was determined by the intersection of the linear regressions of each region. An example is shown in Fig. S1.†

The content of mono-esterified citric acid was determined through complexometric titration with copper sulfate. This titration is based on the technique developed by Menzel *et al.*⁴³ with slight modifications. The principle of the complexometric titration with copper sulfate is that citrate monoesters and copper cations form stable complexes in a ratio of 1:1.⁴³ Titrations were performed on samples in sodium form (–COONa). Around 200 mg of sample was diluted into 100 mL of DI water and followed by the addition of some drops of the indicator murexide at 0.2 wt%. A solution of CuSO₄ 0.01 M was added dropwise until a color change from violet to yellow was observed.

The percentage of carboxyl groups from monoester linkages was calculated as:

$$\frac{2 \times \text{citrate monoester content [mmol g}^{-1}\text{]}}{\text{carboxyl content [mmol g}^{-1}\text{]}}$$

Fourier transform infrared spectroscopy (FTIR). FTIR spectra were recorded on a Varian 670-IR spectrometer equipped with an attenuated total reflection (ATR) accessory. The spectra were recorded as the average of 32 scans at a resolution of 2 cm^{–1} in the range of 500–4000 cm^{–1}. All spectra are presented in absorbance mode and normalized against the band associated with the C–O stretch of C6 (~1030 cm^{–1}) using the software Spectragryph 1.2.14.⁴⁴



Nuclear magnetic resonance (NMR) spectroscopy. Magic-angle spinning (MAS) NMR experiments were performed at a magnetic field of 9.4 T (Larmor frequencies of 400.13, and 100.61 MHz for ^1H and ^{13}C , respectively) on a Bruker Avance-III spectrometer. Spectra were recorded with a 4 mm probehead at 14 kHz MAS rate. The ^1H - ^{13}C cross-polarization (CP) experiments involved Hartmann-Hahn matched ^1H and ^{13}C radio-frequency fields applied for a 500 μs contact interval for the cross-polarization step, and 63 kHz SPINAL-64 proton decoupling. 32 768 signal transients with a 2 s relaxation delay were collected for each sample. The ^{13}C chemical shifts were referenced to tetramethylsilane (TMS). The cellulose crystallinity index (CI) of each of the measured samples was assessed with the spectra deconvolution approach based on the separation of C4 carbon signals of crystalline (~ 89 ppm) and amorphous (~ 84 ppm) phase.^{45,46} CI was calculated by relating the signal intensity (integral) of the C4 signal in the crystalline phase to the total fitted C4 signal intensity of the sample. Spectra were fitted with one Lorentzian for each respective cellulose carbon signal in the spectrum (C1–C6), and one Lorentzian for each amorphous C4 and C6 component in the spectrum (8 functions in total). Although the two-phase crystalline-amorphous model of the cellulose structure is a simplified one, as the paracrystalline and transition regions are not explicitly addressed, it is useful for routine analyses when due to the significantly disordered nature of the material resulting in relatively broad and overlapping signals (as herein), more detailed analyses by NMR spectral fitting are not feasible.⁴⁷

DFT calculations. Models of three different configurations were considered: monoester citrate, diester citrate linked to the same cellulose chain (type I), and diester citrate linked to neighboring AGU units from different polymers chains (type II); see Fig. 5. Calculations were performed with the ORCA code.^{48,49} Geometry optimizations of the models and the subsequent (GIAO) NMR shifts calculations were performed at the revPBE-D4/pcseg-1 and PBE0/pcSseg-2 levels of theory, respectively, and this protocol was proven robust.⁵⁰ An additional set of NMR shifts was calculated at the M06L/pcSseg-2 level of theory for the same models, and the correlation between the two data sets is excellent; see Fig. S2.† CO_2 molecule in the gas phase was used as a chemical shift ref. 51.

Differential scanning calorimetry. The thermal behavior of the recovered citric acid was studied using a differential scanning calorimeter (DSC, Netzsch DSC 214 Polyma) under nitrogen atmosphere. Around 20 mg of sample were sealed in an aluminum crucible with pierced lid. The sample was heated from T_{amb} to 80 $^{\circ}\text{C}$ at a rate of 10 $^{\circ}\text{C min}^{-1}$, isothermal for 5 min, and then heated from 80 $^{\circ}\text{C}$ to 180 $^{\circ}\text{C}$ at a rate of 5 $^{\circ}\text{C min}^{-1}$.

Life cycle assessment

The life cycle assessment was performed according to the guidelines provided by the standards ISO 14040 and ISO 14044. This study is an attributional screening and mapping analysis of CNC preparation at a laboratory scale similar to the work of Piccinno *et al.*²⁵ In this work we explore (1) the environmental

impact of post-consumer cotton over wood pulp as raw material for CNC extraction and (2) the environmental impacts of lab-scale routes for CNC extraction. Three different CNC preparation scenarios were assessed: (S1) CNC prepared from wood pulp by sulfuric acid hydrolysis,^{52,53} (S2) CNC prepared from post-consumer cotton by sulfuric acid hydrolysis,¹⁷ and (S3) CNC prepared from post-consumer cotton by citric acid functionalization and subsequent fibrillation (this work). For the post-consumer cotton, the cut-off allocation was applied meaning that recycled material can be used without burden (up to the recycling process) since the production (*e.g.*, cultivation, harvesting, and processing) of the material is allocated to the first use of the material. This is in line with the “polluter pays principle” in the Environmental Product Declaration (EPD system) and the boundary between the life cycles is defined as the point where the product has its lowest market value.⁵⁴ The functional unit of the study is 1 gram of CNC as an aqueous dispersion. Flowcharts describing the studied systems are shown in ESI (Fig. S3†). For the post-consumer cotton, the system boundaries exclude collecting and transportation, regarding this as part of the previous life cycle stage (cut-off).

The post-consumer cotton was collected and sorted at Wargön Innovation which is located on the Swedish west coast. The textiles that are transported to the Wargön pilot facility are from Röda Korset shops on the Swedish West coast and have been collected *via* manned collection points. At Wargön, the textiles are sorted into three different sorting fractions: (1) textiles that can be re-used (2) textiles that can be used as feedstock for producing new fibers or in new applications (recycling) (3) textiles that need to be incinerated due to contamination. The textiles are sorted both manually and automatically by a conveyor belt with paddles that put the textiles in the right container (for textile recycling a NIR detector is activated to sort fiber blends). The electricity from the conveyor belt was used in the LCA.

Packaging and material flow for the laboratory equipment was not considered at any point during this stage of the study. The main sources of data about the relevant preparation routes are from this and our previous works.^{17,53} The other source of data is the Ecoinvent database (version 3.8), from which inventory data for upstream manufacturing data for pulp, chemicals, water, and electricity has been obtained using the inventory database provided within SimaPro Version 9.3. Life cycle inventory data can be found in ESI (Table S1†). Since the CNC preparation takes place in water, the fugitive emission of volatile organic compounds is assumed to be negligible. However, a sensitivity analysis was performed assuming 100% emission to water of the worst chemical, in this case corresponding to sulfuric acid according to Piccinno *et al.*⁵⁵

Information about background processes and data sources can be found in ESI (Section background processes and Table S2†). The system has been modeled in SimaPro (9.3), which is an LCA software in which the environmental impact of the system could be calculated. The environmental footprint (EF) methodology has been used (LCIA EF3.0) for impact assessment to provide a wide array of impact categories. See ESI for background processes, contribution analysis, and sensitivity



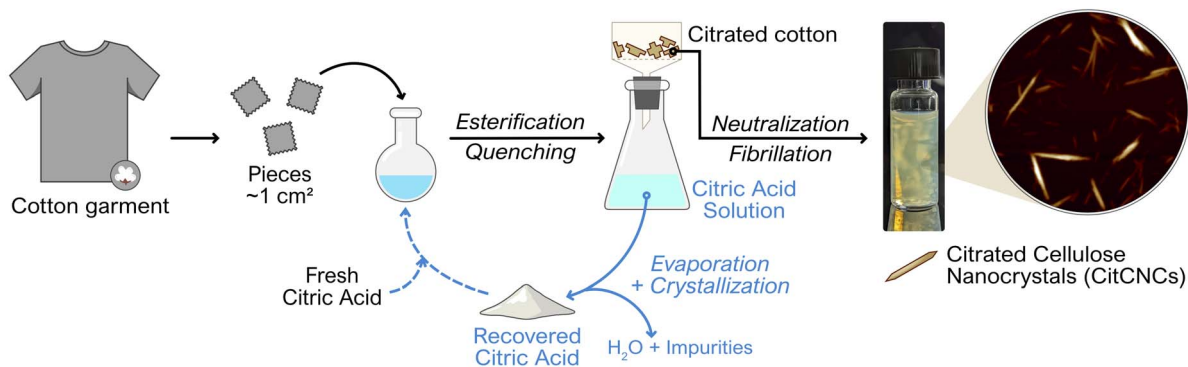


Fig. 1 Schematic illustration of CitCNCs preparation via functionalization with citric acid followed by mechanical fibrillation. Aqueous suspensions of CitCNCs show flow birefringence under cross polarizers.

analysis (see ESI section background processes and guiding process development by LCA).†

Results and discussion

Cellulose nanocrystals with carboxylic moieties were prepared from post-consumer textiles in two main steps (Fig. 1). First, the surface of the cotton was esterified with citric acid, and then the citrated cotton was mechanically fibrillated, while the unreacted citric acid was recovered by evaporation–crystallization.

Preparation of citrated cotton

Cellulose nanoparticles tend to aggregate due to the attractive interactions between their surface hydroxyl groups,⁵⁶ but it can be avoided by introducing charged groups on the nanoparticle surface.⁵⁷ Here, carboxylate groups were introduced on the surface of cotton fabrics before fibrillation by esterifying the cotton with the tricarboxylic citric acid. Optimization experiments (Table S3†) indicated that a high concentration of citric acid and high temperature are needed to achieve a high surface charge on the resulting nanocrystals. This trend was also reported by Ji *et al.* for citrated-CNMs extracted from bleached sugarcane bagasse pulp.³⁶ Nevertheless, some water is essential

to ensure that cellulose hydrolysis will occur simultaneously with the esterification.^{31,58} A correlation between high charge and smaller fibrils was observed (Fig. 2), and we hypothesize that this size reduction facilitates the fibrillation of citrated cotton. Therefore, we performed subsequent reactions at the maximum temperature and concentration of citric acid we could achieve, *i.e.*, saturated (85 wt% (ref. 59)) aqueous citric acid at 100 °C. Under these conditions, a carboxylate content of approximately 1.1 mmol g^{−1} was achieved after 7 h (Table S3†). Although the particle size of the cotton pieces decreased substantially, most citrated cotton existed as fibers with sizes in the micron scale (Fig. 2), as the weak citric acid ($pK_{a1} = 3.135$ at 100 °C (ref. 60)) was insufficient to catalyze the hydrolyzation of all the fibers to nanoparticles.

Both starting cotton fabrics and resultant citrated cotton were analyzed by FTIR. IR spectroscopy (Fig. 3, Table S4†) provided information on the post-consumer cotton fabrics and their interaction with citric acid. The spectrum of the cotton fabrics (I) showed the typical characteristic peaks of pure cellulose, and some small extra peaks corresponding to the stretching of $-\text{CH}_2-$ groups in the region 2800–3000 cm^{−1}.⁶¹ These peaks indicate that impurities with alkyl groups, such as fatty acids, were impregnated on the cotton fabrics during their use as garments. For example, similar peaks, but with higher

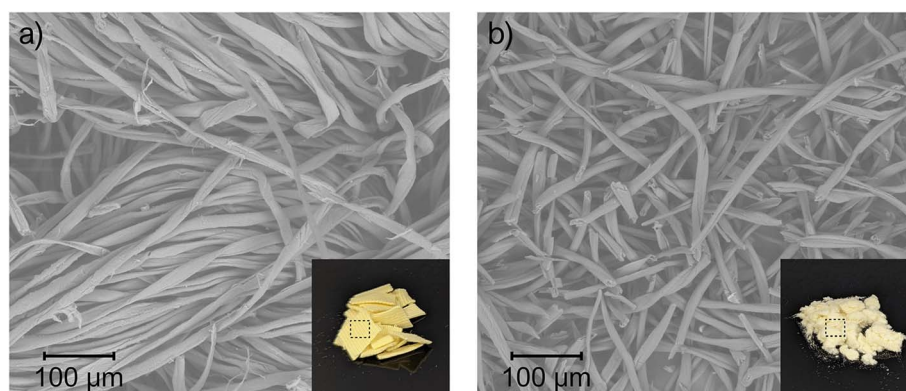


Fig. 2 Morphology of cotton pieces before and after treatment with citric acid. SEM images of cotton fabrics before (a) and after (b) treatment with citric acid. Inset: Photographs of the corresponding cotton pieces.



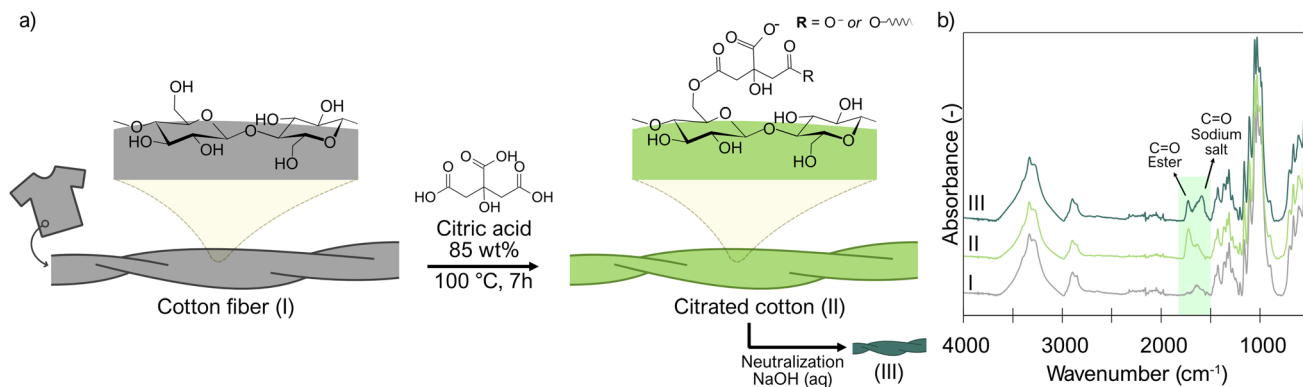


Fig. 3 Esterification of post-consumer cotton pieces. (a) Scheme functionalization of cotton fibers through esterification with citric acid. Cotton pieces reacted with citric acid 85 wt% at 100 °C for 7 h. (b) FTIR spectrum showing the ester bond formed ($\lambda = 1725 \text{ cm}^{-1}$) after functionalization, and the carboxylic moieties as sodium carboxylate salts ($\lambda = 1590 \text{ cm}^{-1}$) after neutralization.

intensity, have been observed in non-scoured cotton due to waxes.^{62,63}

The FTIR of the citrated cotton (II) shows a broad peak in the range $1670\text{--}1770 \text{ cm}^{-1}$ corresponding to the $\text{C}=\text{O}$ stretching vibration band^{64,64} (Fig. 3). After neutralization of the citrated cotton with NaOH (III), it was possible to differentiate between the signals of the carboxyl groups that were present as salts (the band centered at 1590 cm^{-1} corresponds to the asymmetric stretching of $-\text{CO}_2^-$ group⁶¹), and those that were part of ester linkages to the cotton (centered at 1725 cm^{-1} ester $\text{C}=\text{O}$ vibrations⁶¹). These two peaks suggested that the esterification of cellulose was successful and that the carboxyl groups are covalently bonded to cotton. Hence, no pretreatments on cotton fabrics were needed for a successful functionalization, which is a significant advantage since most of the feedstocks used for the extraction of carboxylated CNCs require bleach processing prior to hydrolysis.⁶⁵ Although our reaction is not regioselective, there is a larger preference for the esterification of cellulose with citric acid at the C6 position.³¹

The formation of diesters during the esterification of cellulose with citric acid is also sterically possible. Quantitative estimation of the diester content can be done by titrating the citrated cotton in sodium form with Cu^{2+} . The citrate monoester content was around 0.35 mmol g^{-1} (Table S5†). Hence, carboxylic groups on the citrated cotton are a mixture of monoesters and diesters (Fig. 3a). So, from the total carboxylate charge of 1.1 mmol g^{-1} , around 63% of the carboxylic groups are from monoesters linkages and 37% from diesters. The fact that mechanical fibrillation was possible to occur resulting in colloiddally stable CNCs, suggests that most likely these diesters are formed between neighboring AGU monomers from the same polymer chain or cellulose chains within the same nanofibril since esterification between neighboring nanofibrils would lead to restrained fibrillation and aggregation.

Fibrillation to give CitCNCs

CitCNCs were prepared from citrated cotton by fibrillating with a microfluidizer. To prevent clogging of the machine, cotton-citrated suspensions were treated with a high-shear mixer

before fibrillation. Fibrillation then proceeded for ten passes until no aggregates were observed by the naked eye. The percentage of monoesters on CitCNCs and neutralized citrated cotton were roughly identical (see Table S5†) and there were no significant differences in their FTIR spectra (Fig. S4†). As a reference, CNCs were also extracted from cotton textiles through sulfuric acid hydrolysis (SCNCs) as described in our previous work,¹⁷ and their properties were compared with the properties of CitCNCs.

Size and morphology. Measurements made on at least 200 individual nanoparticles on AFM images of CitCNCs and SCNCs (Fig. 4) indicated average lengths of $L_{\text{SCNCs}} = 150 \pm 55 \text{ nm}$ and $L_{\text{CitCNCs}} = 218 \pm 112 \text{ nm}$, and average heights of $H_{\text{SCNCs}} = 7 \pm 3 \text{ nm}$ and $H_{\text{CitCNCs}} = 12 \pm 7 \text{ nm}$. In general, CNCs extracted from cotton are shorter than CNCs extracted from wood or tunicates.⁶⁶ Both types of extracted CNCs show a rod-like morphology with an aspect ratio of 20 for CitCNCs and 24 for SCNCs. Although CitCNCs were obtained after mechanical treatment, they are referred to as nanocrystals instead of nanofibrils due to their rod-like aspect ratio¹² and high crystallinity (see below).

Overall, CitCNCs are more polydisperse than SCNCs. A broader height distribution implies that a fraction of CitCNCs was not made of elementary fibrils and that some bundles were still present after fibrillation. However, the mechanical treatment performed on citrated cotton hasn't been optimized, and an increment in the number of passes, or methods such as centrifugal fractionation (previously used on other CNMs⁶⁷) could reduce the polydispersity of CitCNCs.

The yield of fibrillation of cotton fabrics into CitCNCs was 78% (Table 1), which is the range of other CNM yields from methods involving functionalization and subsequent mechanical treatment.¹⁰ After 10 passes, the nanoscale fraction of citrated cotton was separated from the microscale fraction using a $0.7 \mu\text{m}$ filter. 82% of the citrated cotton fed into the microfluidizer was fibrillated to the nanoscale.

The esterification of cotton with citric acid allows the grafting of carboxylic groups distributed over the CNC surface. Conductometric and complexometric titrations showed that



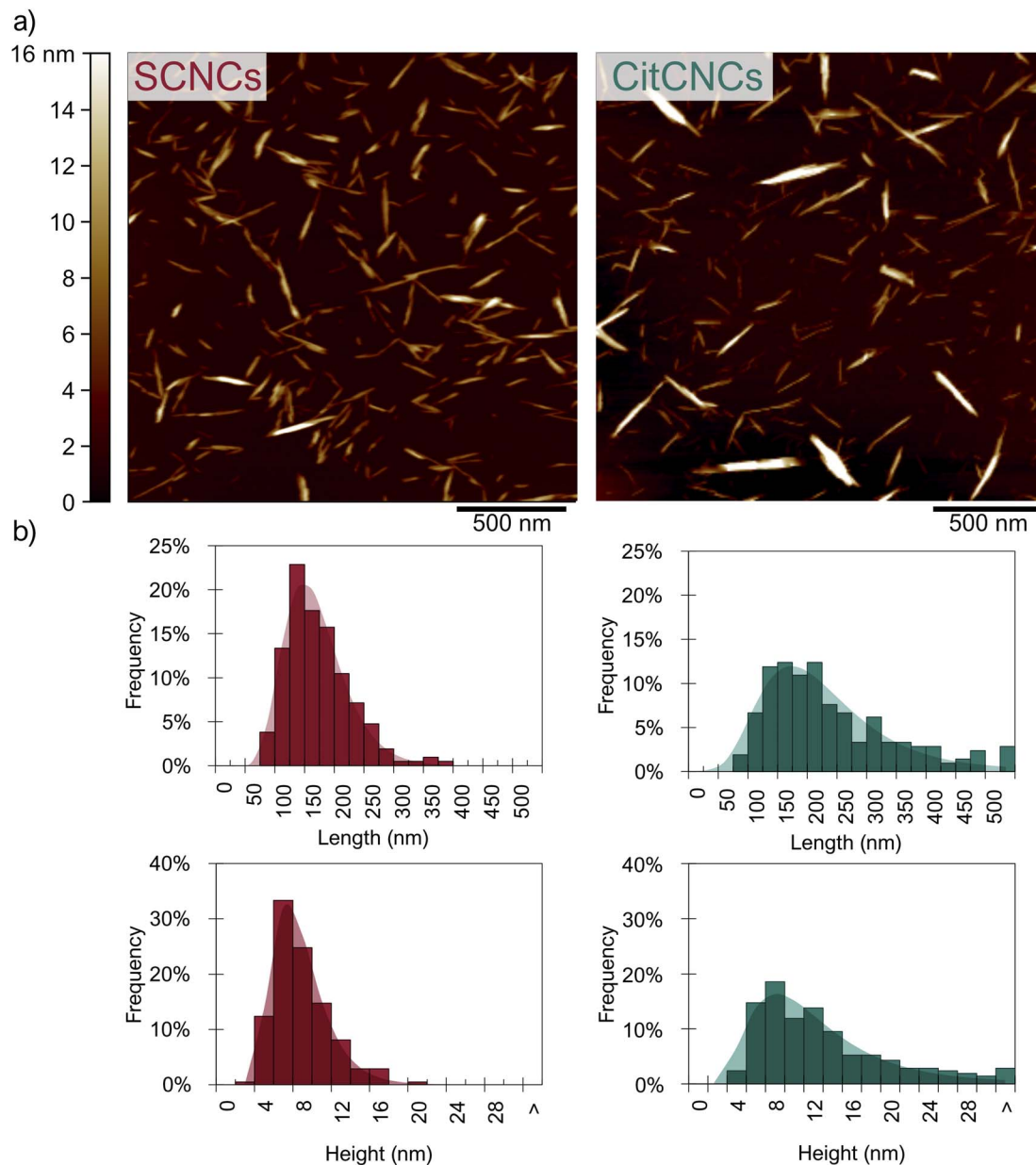


Fig. 4 Comparison of size and morphology of extracted CNCs. (a) $2\ \mu\text{m} \times 2\ \mu\text{m}$ Atomic Force Microscopy images of SCNCs and CitCNCs displayed with the same scale along the z-axis (b) Histograms of length and height distributions of SCNCs and CitCNCs built from at least 200 isolated CNCs.

those groups are covalently bound to cellulose by either mono or diester linkages. Solid-state ^{13}C NMR spectra of cotton and extracted CNCs are shown in Fig. S5.† Spectra show the typical signals of cellulose, as well as a minor signal at 30 ppm, which could correspond to aliphatic carbon chains from the impurities attached to the textiles. For CitCNCs, two additional signals in 40–50 ppm and 165–185 ppm spectral regions are observed and originate from the esterification with citric acid. To assess the most probable configurations of cellulose citrate, three cellulose citrate models were considered (Fig. 5), and the ^{13}C chemical shifts were calculated to facilitate direct comparison with the experimental CitCNC spectrum.

The signals in the 40–50 ppm region could be assigned to the CH_2 carbon atoms from the citrate groups, while the signals in the 165–185 ppm region to the carbonyl carbon atoms from the esters and the carboxylate groups. Peaks around 175 ppm also confirm the presence of ester bonds, as the shifts of the carbonyl groups of sodium citrate typically fall around 180 ppm.⁶⁸ By comparison of the experimental ^{13}C NMR spectrum to the computed chemical shifts, we found that most probably a combination of all three types of cellulose citrate is present in the CitCNCs (Fig. 5).

A relatively high CitCNC surface charge content of 0.9 mmol $-\text{COO}^-/\text{g}$ CitCNCs was achieved, which is in the range of other



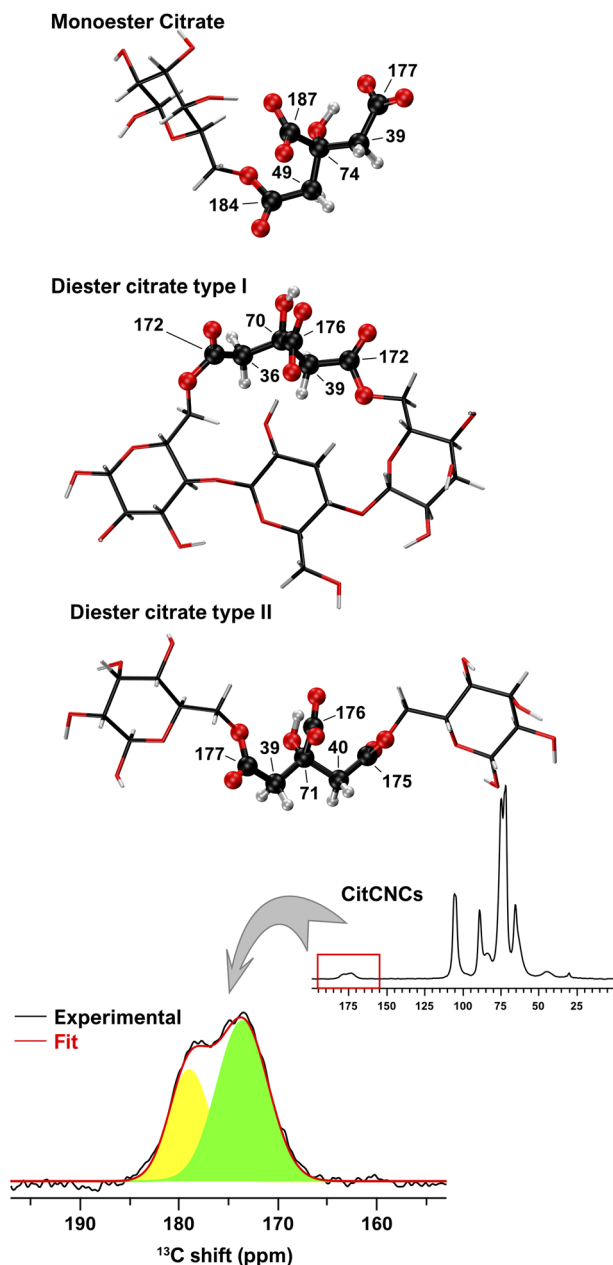


Fig. 5 Structures of cellulose citrate modeled as monoesters or diesters. Each model includes the calculated ^{13}C NMR shifts obtained for each carbon atom of the citrate group. Fitted signal integrals are shown in the bottom panel.

chemical functionalization routes such as TEMPO-catalyzed oxidation,⁶⁹ or esterification with oxalic acid.³⁴ A high surface charge on CNCs not just dictates their colloidal stability⁷⁰ and rheology⁷¹ but also increases the range of applications including electrostatic interactions or complexations, necessary in, for instance, water treatment.

The surface charge and surface chemistry of CitCNCs could make them suitable for a wider range of applications. The carboxylic groups of CitCNCs can undergo chemical modifications not possible for the sulfate-half ester groups in SCNCs. For example, amidation or esterification with alcohols can be

Table 1 Yield and properties of CitCNCs and SCNCs extracted from post-consumer cotton textiles

| Sample | Yield (g CNCs/g cotton) | Surface charge (mmol kg ⁻¹ CNC) | Crystallinity index (%) | |
|---------------------|----------------------------|---|----------------------------|-----|
| | | | XRD | NMR |
| Cotton ^a | — | — | 93 | 62 |
| SCNCs | 61 ± 1% ^b | 276 ± 4 ^b | 90 | 66 |
| CitCNCs | 78 ± 4% | 900 ± 55 | 89 | 62 |

^a Cotton: as received post-consumer cotton textiles. ^b Data from Ruiz-Caldas *et al.*¹⁷

performed on carboxylated CNCs.⁶⁵ Additionally, citrate groups serve as reducing agents, capping agents, and chelating agents, and their interactions can be tailored through pH variations. Citric acid is a widely used organic ligand capable of forming different types of complexes with a variety of metal ions, including elements that are hazardous to the environment such as As and Cr.^{60,72} We believe that these interaction mechanisms could also take place with the surface groups attached to the CitCNCs.

Fig. 6a–c shows the XRD patterns of Cotton and the extracted CNCs and their deconvoluted peaks using Void fittings for the crystalline and amorphous peaks. Peak information can be found in the ESI (Table S6†). Cotton, SCNCs, and CitCNCs show the same characteristic peaks of cellulose I β : 2θ around 14.6° (110), 16.5° (110), 20.4° (012), 22.7° (200), and 34.5° (004).⁷³ Interestingly, the peaks corresponding to the (012) and (004) lattice planes are less visible on the diffractogram of the CNCs, compared to the diffraction pattern of cotton. Most likely, this is due to the CNCs adopting a preferred orientation during sample preparation along the *ab* plane due to their needle-like shape. The peak at 20.4° could also correspond to fractions of mercerized cotton present on the starting cotton fabric⁷⁴ as artifacts of textile finishing.

The chemical and mechanical methods used for the preparation of CitCNCs did not affect the crystalline structure of cotton since the diffraction peaks of cellulose I β are clearly visible on the diffractogram of CitCNCs. Two methods were used for the calculation of the crystallinity index (CI): the XRD deconvolution and the NMR C4 peak separation method.⁴⁵ Daicho *et al.*⁴¹ showed that the CI values obtained by NMR could be lower than values obtained by XRD for the same sample. The initial cotton fabrics and the extracted CNCs have relatively high crystallinity (Table 1) with subtle differences among samples. These differences could be attributed to the uncertainty of the measurement. When substrates with high crystallinities are used for CNC extraction, only slight changes in the CI of the CNCs were observed.⁷⁵ Post-consumer cotton fabrics can be seen as an optimal substrate for the extraction of nanoparticles with high crystallinity as cotton is one of the sources of cellulose with the highest crystallinity among plants.¹⁴ Besides, crystallinity is one of the CNC properties that is mainly dependent on the source of cellulose and cannot be easily tuned through the production route.¹⁰ In addition, Palme *et al.* showed that the CI of cotton is not significantly affected by laundering and use.⁷⁶



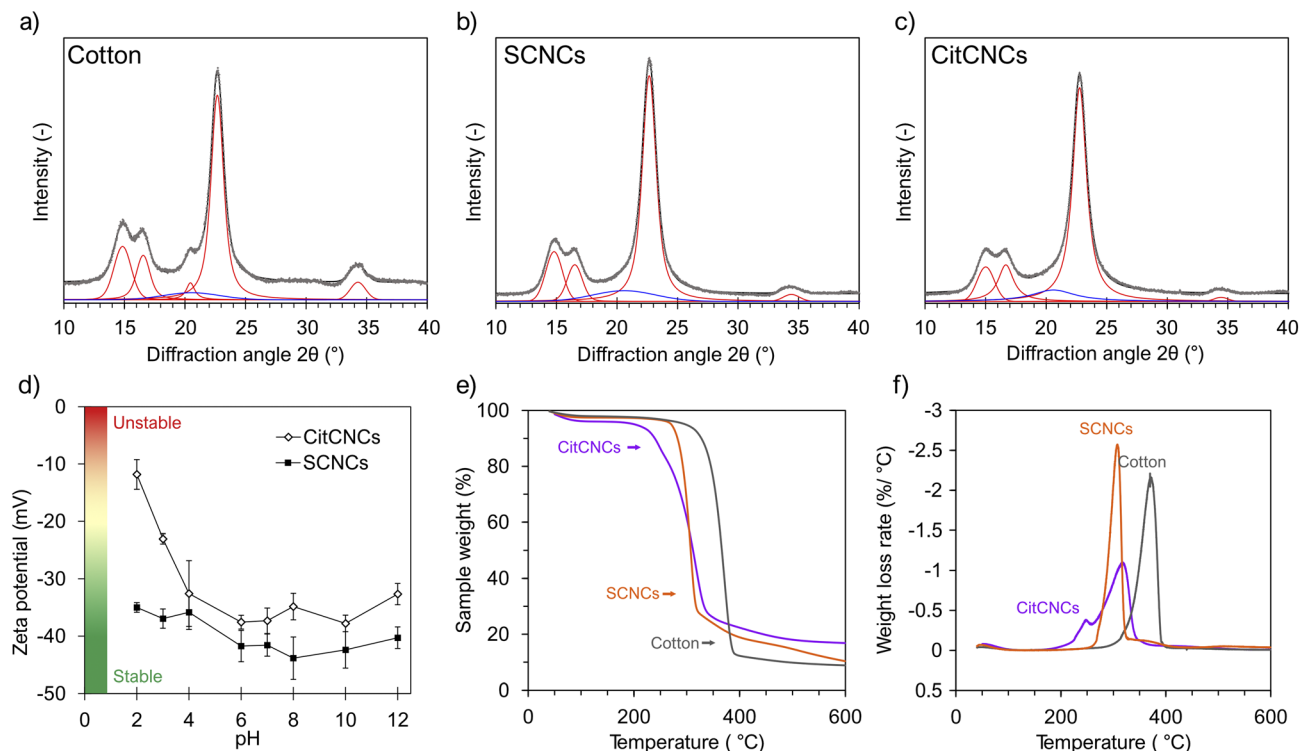


Fig. 6 Properties of cotton textiles and the extracted CNCs. (a–c) XRD profiles from cotton fabrics and extracted cellulose nanocrystals. The dotted curve corresponds to the experimental data. The black line is the fitted model, the red lines are the crystalline peaks, and the blue line is the amorphous peak. (d) Zeta-potential of CNCs in suspension at different pH measured in 1 mM NaCl background electrolyte. Each point is the average with the error bars representing the standard deviation. Thermogravimetric analysis: (e) TGA and (f) DTGA curves of CitCNCs, SCNCs, and cotton.

The average crystallite size was determined with the full width at half maximum (FWHM) of the (200) reflection using the Debye–Scherrer formula. The component of the instrumental broadening was not included in the calculation, so the values obtained represent a lower limit of the crystallite size.⁷⁷ Both CNCs have similar crystallite sizes ($D_{\text{SCNCs}} = 5.8$ nm, $D_{\text{CitCNCs}} = 5.8$ nm) and both values are slightly smaller than the crystallite size of the starting cotton fabrics ($D_{\text{cotton}} = 6.4$ nm). The crystallite size and CI from NMR of cotton fabrics are comparable to values reported in the literature,^{76,78} and the crystallite size of SCNCs is consistent with the number-average height obtained from AFM data (Fig. 4). The differences in the crystallite size could simply be due to the peak-fitting method. The extracted CNCs have lower crystallinity than cotton since smaller crystallite sizes imply lower crystallinity. In the case of SCNCs, the hydrolysis conditions used for their extraction could have affected portions of the crystalline regions as well, while for CitCNCs, other works have shown that mechanical fibrillation decreases the crystallite size.⁴¹

Colloidal stability

Both CNCs display a negative zeta potential across the whole pH range with the lowest ζ -values in the neutral or slightly basic pH range, and the highest ζ at low acidic pH (Fig. 6d). However, SCNCs show colloidal stability over the whole studied pH range while CitCNCs are less stable at low acidic pH. The CNC surface

charge, and thus, their colloidal stability, is dictated by the dissociation equilibrium of the surface groups. SCNCs have sulfate half ester groups on their surfaces,⁷⁹ and the second pK_a of sulfuric acid at 25 °C is 1.99, so the $-\text{OSO}_3^-$ groups should be mainly protonated ($-\text{OSO}_3\text{H}$) below pH 2 and deprotonated at $\text{pH} > 2$.⁸⁰ On the other hand, the pK_a of the remaining carboxyl groups of cellulose citrate are 4.75 and 6.40, so the free carboxylic groups of CitCNCs will be protonated (COOH) below pH 4. One advantage of this pH-dependent condition is that the rheological properties of CitCNCs dispersions could be tailored on less acidic pH conditions. In the pH range where the citrate groups are protonated (COOH), an increase in the elastic modulus and viscosity will occur due to particle aggregation. Similar behavior was described by Facchine *et al.* for nanochitin suspensions.⁸¹

Thermal properties and moisture uptake

The thermal stability of cotton and extracted CNCs were assessed using TGA. Fig. 6e and f show the degradation profiles as well as the mass loss rates. All three samples have small a mass loss at temperatures below 100 °C due to adsorbed water, with CitCNCs having the highest water loss (4 wt%) due to a higher water affinity as a result of the citrate surface groups.⁸² The differences in water loss are consistent with the differences in the moisture uptake observed between SCNCs and CitCNCs (Table 2). For the moisture uptake, the samples



Table 2 Thermal properties of post-consumer cotton textile and the extracted CNCs

| Sample | T_{onset} (°C) | T_{peak} (°C) | DT_{peak} (% wt/°C) | Char residue (%) | Moisture uptake ^a (%) |
|---------|-------------------------|--|--|------------------|----------------------------------|
| Cotton | 333 | 361 | −2.2 | 10 | — |
| SCNCs | 288 | 307 | −2.5 | 11 | 12.2 ± 0.8 |
| CitCNCs | 224 | T_{p_1} = 247 T_{p_2} = 319 | DT_{p_1} = −0.1 DT_{p_2} = −1.1 | 18 | 16.0 ± 0.4 |

^a Measured at a relative humidity of 84 wt% at t = 24 h.

were monitored for two more days, and no significant differences were observed (Fig. S6†).

Their thermal profiles at higher temperatures are significantly different. Cotton pieces show a single and rapid weight drop corresponding to the cellulose degradation involving depolymerization of cellulose, and dehydration and decomposition of glycosyl units.⁸³ The peak temperature (361 °C) and char residue (10%) coincide with values reported in the literature.⁸⁴ Hence, the dyes or other impurities attached to the cotton fabric used in this work do not seem to affect its thermal stability. Nevertheless, darker dyes or other finishes could influence the thermal stability of cotton fabrics.²⁰

SCNCs also have a single sharp weight drop, but their thermal decomposition starts at lower temperatures than cotton. This is a nanoscale effect resulting in an increment of reducing ends that decreases the thermal stability of cellulose.^{85,86} The sulfate half-ester groups on the SCNC surface do not affect the thermal stability of CNCs since they are in sodium form (−OSO₃Na), thus preventing the structural dehydration catalyzed by sulfate groups in acid form.^{87,88} Interestingly, SCNCs from other cotton fabrics have the same thermal profile, independent of the coloration of the starting material. Most likely the concentration of dye and other impurities left after CNC extraction is too low to influence the thermal degradation of CNCs. Another advantage of upcycling textile waste into CNMs is that the differences in the thermal profiles of the

cotton fabrics due to different degrees of polymerization, if present, would not affect the properties of the extracted SCNCs.

The thermogram of CitCNCs shows a two-step decomposition distributed over a wide temperature interval, compared to only a single mass drop observed in cotton and SCNCs. Similar thermal behaviors were reported for other citrated-CNMs.^{36,88} This earlier degradation is presumably due to the decomposition of citric acid which has a visible effect at high surface charges. TEMPO-oxidized CNMs^{10,89} have lower thermal stability than CitCNCs since the carboxyl groups, which lead to accelerated thermal decomposition of cellulose,^{58,86} are not directly attached to the cellulose backbone.⁸⁸

Guiding process development by life cycle assessment

Fig. 7a indicates that the baseline scenario, S1 (SCNC from wood pulp) had a higher environmental impact across all 16 categories (EF 3.0) compared to S2 (SCNC from post-consumer cotton). Detailed results of the environmental assessment are shown in Table S7.† The lower environmental burden of S2 suggests that post-consumer cotton is a promising feedstock for CNC production. From a sustainable perspective, cotton fabrics have the added advantage of not requiring additional purification steps to achieve a high cellulose content, as they inherently have a high cellulose content. However, cotton fabrics may contain unwanted impurities from both their production and

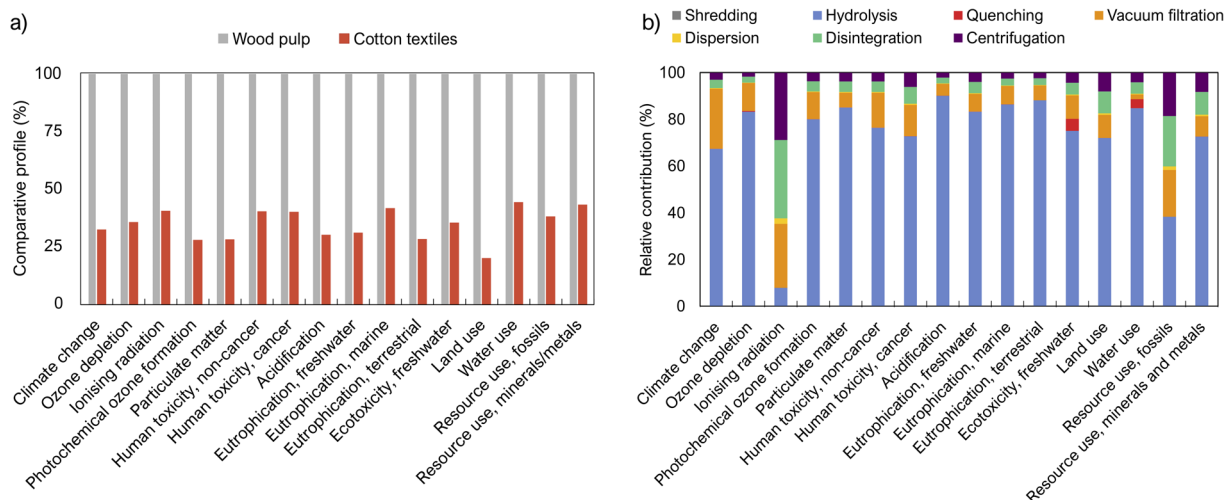


Fig. 7 (a) Comparative environmental profiles for SCNC preparation from wood pulp (S1) and post-consumer cotton textiles (S2). Impacts are normalized to S1. (b) Environmental profile of CitCNC production route.



use, which can potentially limit the field of applications of the extracted CNCs.

Concerning CitCNC extraction (S3), the hydrolysis step was the most dominant contributor (Fig. 7b) due to the usage of citric acid, whose production contributes to all 16 impact categories. A similar finding is reported by Bondancia *et al.*²⁹ A contribution analysis of S1 and S2 can be found in ESI (Fig. S7 and S8†). The largest difference comparing the impact of S3 with the other scenarios (Table S7†) was *eutrophication terrestrial* (release of nutrients to the soil) mainly due to the emission of ammonia, nitrate, nitrogen oxide, and nitrogen monoxide from the citric acid production. The second largest difference was *water use* due to the high amount of water used during the production of citric acid. Another interesting impact category is climate change and, in this category, S3 had a similar climate change impact as S1 which also was surprising. The high climate change impact of S3 is a result of the high contribution of CO₂ fossil due to the higher ratio of citric acid to cotton (compared to sulfuric acid) used during the CNC preparation. Sensitivity analyses for each scenario can be found in ESI (Section Sensitivity analysis, Table S8, and Fig. S7–S9†). The high impact of citric acid can be reduced by decreasing the input amount and improving the acid recovery.

Citric acid recovery and its environmental impact

One of the main challenges of the extraction of CNCs through sulfuric acid hydrolysis is the recovery of unreacted sulfuric acid.⁹⁰ Although the route of CitCNC extraction has a higher environmental impact than SCNC, an advantage of using citric acid is that it can be recrystallized at ambient conditions, and thus separation from sugars and other by-products is feasible. In this work, the first liter of the effluent after quenching was collected for citric acid recovery. After crystallization, solid crystals of citric acid and a saturated solution of citric acid containing most of the impurities were obtained. To increase the amount of citric acid recovered, a few drops of sulfuric acid and approximately 1 g of citric acid was added to the saturated solution following a procedure described before.^{91,92} The solid crystals helped to induce crystallization, while the drops of sulfuric acid reduced the solubility of citric acid due to Le Chatelier's principle. The total percentage of citric acid recovered was 58 ± 4 wt%.

The DSC curve of the recovered solid (Fig. S12†) shows a single and narrow endothermic peak, so the citric acid crystallized in the anhydrous form. It is known from the literature that anhydrous citric acid crystallizes from hot aqueous solutions.⁶⁰ Besides, the monohydrate citric acid has different phase transitions since it gradually loses the water from its structure during heating (Fig. S12†).

The recovered citric acid has a decrease in the melting temperature by 3 °C due to the presence of some impurities. To determine the purity of the recovered citric acid, we considered it an ideal eutectic mixture and used the Schröder-van Laar model. The melting temperature of the recovered citric acid was calculated from the Differential Scanning Calorimetry (DSC) data. Our results showed a purity of 92 ± 1 mol% (see ESI† for

further details). Although this value should be taken as a simple approximation.

We modeled a process that considers the recovery obtained above, and when comparing scenarios, it is evident that a recovery of 58% leads to a much lower environmental impact on all categories, with a drop of up to ~48% in the *water use* category (see Fig. S13†). Even though recovering citric acid involves a heat input, with the decrease in the environmental burden it is worth implementing measures to reduce the usage of citric acid, and thereof, diminish the overall environmental impact of the route developed in this study. The yield of 58% from this study is lower than the reported yield for the same method of concentration followed by sulfuric acid addition (>80% (ref. 91 and 92)), and other methods such as precipitation (65–93% (ref. 93)) and concentration followed by solvent extraction (90% (ref. 94)) to name a few. Most likely not all the available citric acid was present in the effluent collected. Nevertheless, this means there is an opportunity to reduce the environmental burden by improving the yield and reevaluating the environmental impact with the new mass and energy balances.

Conclusions

This work shows a catalyst-free route for the extraction of carboxylated CNCs (CitCNCs) from real post-consumer cotton-based fabrics. The proposed route involves the surface esterification of cotton with citric acid followed by mechanical fibrillation. The optimal conditions for the functionalization of cotton were achieved at a concentration of citric acid of 85 wt% and a temperature of 100 °C. FTIR and ¹³C NMR spectra confirmed the partial esterification of the cotton fabrics while conductometric and complexometric titrations showed that the free carboxylic groups are chemically attached to the cotton surface by mono or diester bonds. DFT theoretical calculations confirmed the presence of both mono and diesters of citric acid and suggest that citrate diesters could be bonded to the same polymer chain or between neighboring AGU units. The successful functionalization of discarded cotton fabrics without the need for chemical pretreatments highlights the potential of these materials as an alternative to refined cellulosic feedstocks for the preparation of CNCs.

Citrated cotton was mechanically fibrillated to produce CitCNCs with a mass recovery of 78% (g CitCNCs/g cotton). The ability to extract CNCs in high yield without the need for pretreatments is a great advantage in terms of sustainability and costs. Furthermore, discarded cotton fabrics are a world-wide available and inexpensive feedstock, making them a readily accessible cellulosic source for CNC extraction.

The size of the obtained CitCNCs was 12 ± 7 nm in height and 218 ± 112 nm in length. These nanoparticles showed good colloidal stability in the pH range of 4–12, similar crystallinity to CNCs extracted from hydrolysis with sulfuric acid, and a high surface charge of 0.9 mmol g^{-1} .

Here we also show how early LCA studies can be useful for understanding and improving the environmental performance of lab-scale routes, essential information for future scale-up.



LCA showed that post-consumer cotton could be a promising feedstock for the extraction of CNCs since its environmental burden is lower than using wood pulp. Nevertheless, post-consumer cotton garments could contain harmful substances from their first lifecycle which need to be further assessed.

Although CitCNC had higher environmental impacts than SCNC in an initial setup, mainly due to the upstream processes of citric acid, the high yield, and the properties of CitCNCs encourage the development of more efficient routes for the recovery of citric acid. The current 58% recovery of citric acid by simple evaporation and crystallization already reduces their environmental impact and sets the foundation for a more environmental-friendly process that can be further improved.

We present a route for the conversion of real post-consumer cotton fabrics into high-quality CNCs, which could be an attractive alternative for the valorization of cotton fabrics. This route could also be used on cotton fibers that are not suitable for spinning and nowadays are considered waste. Future optimization on the amount of citric acid used, the number of passes on the microfluidizer, and the yield of recovered citric acid could reduce the environmental impact of CitCNC production. CitCNCs can be used on multiple advanced applications that can benefit from their size, crystallinity, aspect ratio and surface charge and chemistry, such as water purification and reinforcement materials.

Author contributions

Maria-Ximena Ruiz-Caldas: conceptualization, methodology, formal analysis, investigation, visualization, writing – original draft. Varvara Apostolopoulou-Kalkavoura: conceptualization, investigation, methodology, validation, writing – original draft. Anna-Karin Hellström: conceptualization, methodology, formal analysis, writing – review & editing. Jutta Hildenbrand: conceptualization, methodology, writing – review & editing. Mikael Larsson: conceptualization, methodology, formal analysis, writing – review & editing. Aleksander Jaworski: validation, investigation, methodology, validation, visualization. Joseph S. M. Samec: conceptualization, writing – review & editing, supervision. Panu Lahtinen: resources, writing – review & editing. Tekla Tammelin: resources, writing – review & editing. Aji P. Mathew: conceptualization, funding acquisition, resources, writing – review & editing, supervision.

Conflicts of interest

The authors declare no competing financial interest.

Acknowledgements

The authors thank the Swedish Foundation for Strategic Environmental Research (Mistra: project Mistra SafeChem, project number 2018/11) and Formas 2021-00440 for financial support. This research was also partially sponsored by XPRES (Centre of Excellence in Production Research) – a strategic research area in Sweden. Open-access publication was funded by Stockholm University Library. The authors would like to thank Wargön

Innovation for providing textile samples, Marlene Viertler from the Technical University of Munich for the acquisition of SEM images, and Dr Tamara Church for fruitful discussions. This work was part of the Academy of Finland Flagship Programme Competence Center for Materials Bioeconomy, FinnCERES.

References

- 1 R. Shishoo, Introduction: trends in the global textile industry, in *The Global Textile and Clothing*, Industry Elsevier, 2012, pp. 1–7.
- 2 B. Piribauer and A. Bartl, Textile recycling processes, state of the art and current developments: a mini review, *Waste Manage. Res.*, 2019, **37**, 112–119.
- 3 European Topic Centre on Waste and Materials in a Green Economy, Textiles and the environment in a circular economy, *Eionet Report-ETC/WMGE*, 2019, vol. 6.
- 4 Ellen MacArthur Foundation, *A New Textiles Economy: Redesigning Fashion's Future*, 2017.
- 5 *Preferred Fiber & Materials Market Report 2021*, 2021.
- 6 F. A. Esteve-Turrillas and M. de la Guardia, Environmental impact of recover cotton in textile industry, *Resour., Conserv. Recycl.*, 2017, **116**, 107–115.
- 7 B. Thomas, M. C. Raj, K. B. Athira, *et al.*, Nanocellulose, a Versatile Green Platform: From Biosources to Materials and Their Applications, *Chem. Rev.*, 2018, **118**, 11575–11625.
- 8 D. Klemm, F. Kramer, S. Moritz, *et al.*, Nanocelluloses: A New Family of Nature-Based Materials, *Angew. Chem., Int. Ed.*, 2011, **50**, 5438–5466.
- 9 T. Li, C. Chen, A. H. Brozena, *et al.*, Developing fibrillated cellulose as a sustainable technological material, *Nature*, 2021, **590**, 47–56.
- 10 O. M. Vanderfleet and E. D. Cranston, Production routes to tailor the performance of cellulose nanocrystals, *Nat. Rev. Mater.*, 2021, **6**, 124–144.
- 11 D. Trache, A. F. Tarchoun, M. Derradji, *et al.*, Nanocellulose: From Fundamentals to Advanced Applications, *Front. Chem.*, 2020, **8**, 392.
- 12 S. J. Eichhorn, A. Etale, J. Wang, *et al.*, Current international research into cellulose as a functional nanomaterial for advanced applications, *J. Mater. Sci.*, 2022, **57**, 5697–5767.
- 13 M. Sfiligoj Smole, S. Hribernik, M. Kurečić, A. Urbanek Krajnc, T. Kreže and K. Stana Kleinschek, *Cellulose Nanofibres*, 2019, pp. 61–71.
- 14 H. Krässig, J. Schurz, R. G. Steadman, *et al.*, Cellulose, in *Ullmann's Encyclopedia of Industrial Chemistry*, Wiley, 2004.
- 15 Appendix, in *Wood Chemistry*, Elsevier, 1993, p. 249.
- 16 Y. L. Hsieh, Chemical structure and properties of cotton, in *Cotton*, Elsevier, 2007, pp. 3–34.
- 17 M.-X. Ruiz-Caldas, J. Carlsson, I. Sadiktsis, A. Jaworski, U. Nilsson and A. P. Mathew, Cellulose Nanocrystals from Postconsumer Cotton and Blended Fabrics: A Study on Their Properties, Chemical Composition, and Process Efficiency, *ACS Sustainable Chem. Eng.*, 2022, **10**, 3787–3798.
- 18 K. S. Prado, D. Gonzales and M. A. S. Spinacé, Recycling of viscose yarn waste through one-step extraction of nanocellulose, *Int. J. Biol. Macromol.*, 2019, **136**, 729–737.



- 19 S. Huang, R. Tao, A. Ismail and Y. Wang, Cellulose Nanocrystals Derived from Textile Waste through Acid Hydrolysis and Oxidation as Reinforcing Agent of Soy Protein Film, *Polymers*, 2020, **12**, 958.
- 20 T. Zhong, R. Dhandapani, D. Liang, *et al.*, Nanocellulose from recycled indigo-dyed denim fabric and its application in composite films, *Carbohydr. Polym.*, 2020, **240**, 116283.
- 21 C. Tanaka, Y. Yui and A. Isogai, TEMPO-Mediated Oxidation of Cotton Cellulose Fabrics with Sodium Dichloroisocyanurate, *J. Fiber Sci. Technol.*, 2016, **72**, 172–178.
- 22 I. A. Carrete, P. A. Quiñonez, D. Bermudez and D. A. Roberson, Incorporating Textile-Derived Cellulose Fibers for the Strengthening of Recycled Polyethylene Terephthalate for 3D Printing Feedstock Materials, *J. Polym. Environ.*, 2021, **29**, 662–671.
- 23 International Organisation for Standardization, *ISO 14040—Environmental Management—Life Cycle Assessment—Principles and Framework*, Geneva, 2006.
- 24 Ö. Ögmundarson, M. J. Herrgård, J. Forster, M. Z. Hauschild and P. Fantke, Addressing environmental sustainability of biochemicals, *Nat. Sustain.*, 2020, **3**, 167–174.
- 25 F. Piccinno, R. Hischer, S. Seeger and C. Som, Life Cycle Assessment of a New Technology To Extract, Functionalize and Orient Cellulose Nanofibers from Food Waste, *ACS Sustainable Chem. Eng.*, 2015, **3**, 1047–1055.
- 26 Q. Li, S. McGinnis, C. Sydnor, A. Wong and S. Rennecker, Nanocellulose Life Cycle Assessment, *ACS Sustainable Chem. Eng.*, 2013, **1**, 919–928.
- 27 R. Arvidsson, D. Nguyen and M. Svanström, Life Cycle Assessment of Cellulose Nanofibrils Production by Mechanical Treatment and Two Different Pretreatment Processes, *Environ. Sci. Technol.*, 2015, **49**, 6881–6890.
- 28 L. Tan, S. J. Mandley, W. Peijnenburg, *et al.*, Combining ex-ante LCA and EHS screening to assist green design: a case study of cellulose nanocrystal foam, *J. Cleaner Prod.*, 2018, **178**, 494–506.
- 29 T. J. Bondancia, G. Batista, J. de Aguiar, *et al.*, Cellulose Nanocrystals from Sugar Cane Bagasse Using Organic and/or Inorganic Acids: Techno-Economic Analysis and Life Cycle Assessment, *ACS Sustainable Chem. Eng.*, 2022, **10**, 4660–4676.
- 30 R. M. Leão, P. C. Miléo, J. M. L. L. Maia and S. M. Luz, Environmental and technical feasibility of cellulose nanocrystal manufacturing from sugarcane bagasse, *Carbohydr. Polym.*, 2017, **175**, 518–529.
- 31 I. Romeo, F. Olivito, A. Tursi, *et al.*, Totally green cellulose conversion into bio-oil and cellulose citrate using molten citric acid in an open system: synthesis, characterization and computational investigation of reaction mechanisms, *RSC Adv.*, 2020, **10**, 34738–34751.
- 32 G. P. Touey and J. E. Kiefer, Cellulose citrates and their preparation, *US Pat.*, US2759787A, 1956.
- 33 L. Chen, J. Y. Zhu, C. Baez, P. Kitin and T. Elder, Highly thermal-stable and functional cellulose nanocrystals and nanofibrils produced using fully recyclable organic acids, *Green Chem.*, 2016, **18**, 3835–3843.
- 34 D. Li, J. Henschen and M. Ek, Esterification and hydrolysis of cellulose using oxalic acid dihydrate in a solvent-free reaction suitable for preparation of surface-functionalised cellulose nanocrystals with high yield, *Green Chem.*, 2017, **19**, 5564–5567.
- 35 W. Liu, H. Du, H. Liu, *et al.*, Highly Efficient and Sustainable Preparation of Carboxylic and Thermostable Cellulose Nanocrystals via FeCl₃-Catalyzed Innocuous Citric Acid Hydrolysis, *ACS Sustainable Chem. Eng.*, 2020, **8**, 16691–16700.
- 36 H. Ji, Z. Xiang, H. Qi, T. Han, A. Pranovich and T. Song, Strategy towards one-step preparation of carboxylic cellulose nanocrystals and nanofibrils with high yield, carboxylation and highly stable dispersibility using innocuous citric acid, *Green Chem.*, 2019, **21**, 1956–1964.
- 37 K. J. Nagarajan, A. N. Balaji, S. T. Kasi Rajan and N. R. Ramanujam, Preparation of bio-eco based cellulose nanomaterials from used disposal paper cups through citric acid hydrolysis, *Carbohydr. Polym.*, 2020, **235**, 115997.
- 38 T. J. Bondancia, J. de Aguiar, G. Batista, *et al.*, Production of Nanocellulose Using Citric Acid in a Biorefinery Concept: Effect of the Hydrolysis Reaction Time and Techno-Economic Analysis, *Ind. Eng. Chem. Res.*, 2020, **59**, 11505–11516.
- 39 H.-Y. Yu, D.-Z. Zhang, F.-F. Lu and J. Yao, New Approach for Single-Step Extraction of Carboxylated Cellulose Nanocrystals for Their Use As Adsorbents and Flocculants, *ACS Sustainable Chem. Eng.*, 2016, **4**, 2632–2643.
- 40 H. Yu, S. Y. H. Abdalkarim, H. Zhang, C. Wang and K. C. Tam, Simple Process To Produce High-Yield Cellulose Nanocrystals Using Recyclable Citric/Hydrochloric Acids, *ACS Sustainable Chem. Eng.*, 2019, **7**, 4912–4923.
- 41 K. Daicho, T. Saito, S. Fujisawa and A. Isogai, The Crystallinity of Nanocellulose: Dispersion-Induced Disorder of the Grain Boundary in Biologically Structured Cellulose, *ACS Appl. Nano Mater.*, 2018, **1**, 5774–5785.
- 42 M. Wojdyr, Fityk: a general-purpose peak fitting program, *J. Appl. Crystallogr.*, 2010, **43**, 1126–1128.
- 43 C. Menzel, E. Olsson, T. S. Plivelic, *et al.*, Molecular structure of citric acid cross-linked starch films, *Carbohydr. Polym.*, 2013, **96**, 270–276.
- 44 F. Menges, *Spectragryph - Optical Spectroscopy Software*, Version 1.2.14, v1.2.14, 2020.
- 45 S. Park, J. O. Baker, M. E. Himmel, P. A. Parilla and D. K. Johnson, Cellulose crystallinity index: measurement techniques and their impact on interpreting cellulase performance, *Biotechnol. Biofuels*, 2010, **3**, 10.
- 46 R. H. Atalla and D. L. VanderHart, The role of solid state NMR spectroscopy in studies of the nature of native celluloses, *Solid State Nucl. Magn. Reson.*, 1999, **15**, 1–19.
- 47 P. T. Larsson, K. Wickholm and T. Iversen, A CP/MAS13C NMR investigation of molecular ordering in celluloses, *Carbohydr. Res.*, 1997, **302**, 19–25.
- 48 F. Neese, The ORCA program system, *Wiley Interdiscip. Rev. Comput. Mol. Sci.*, 2012, **2**, 73–78.



- 49 F. Neese, F. Wennmohs, U. Becker and C. Riplinger, The ORCA quantum chemistry program package, *J. Chem. Phys.*, 2020, **152**, 224108.
- 50 A. Jaworski and N. Hedin, Local energy decomposition analysis and molecular properties of encapsulated methane in fullerene ($\text{CH}_4@C_{60}$), *Phys. Chem. Chem. Phys.*, 2021, **23**, 21554–21567.
- 51 P. Rzepka, Z. Bacsik, A. J. Pell, N. Hedin and A. Jaworski, Nature of Chemisorbed CO_2 in Zeolite A, *J. Phys. Chem. C*, 2019, **123**, 21497–21503.
- 52 K. M. Vanhatalo and O. P. Dahl, Effect of mild acid hydrolysis parameters on properties of microcrystalline cellulose, *Bioresources*, 2014, **9**, 4729–4740.
- 53 D. Bondeson, A. Mathew and K. Oksman, Optimization of the isolation of nanocrystals from microcrystalline cellulose by acid hydrolysis, *Cellulose*, 2006, **13**, 171–180.
- 54 EPD International, *General Programme Instructions for the International EPD® System*, Version 4.0, Stockholm, Sweden, 2021.
- 55 F. Piccinno, R. Hischier, S. Seeger and C. Som, From laboratory to industrial scale: a scale-up framework for chemical processes in life cycle assessment studies, *J. Cleaner Prod.*, 2016, **135**, 1085–1097.
- 56 A. Dufresne, Nanocellulose: a new ageless bionanomaterial, *Mater. Today*, 2013, **16**, 220–227.
- 57 P. Lu and Y. I. Hsieh, Preparation and properties of cellulose nanocrystals: Rods, spheres, and network, *Carbohydr. Polym.*, 2010, **82**, 329–336.
- 58 D. Klemm, B. Philipp, T. Heinze, U. Heinze and W. Wagenknecht, General Considerations on Structure and Reactivity of Cellulose: Section 2.3–2.3.7, in *Comprehensive Cellulose Chemistry*, Wiley, 1998, pp. 83–129.
- 59 L. H. Dalman, The Solubility of Citric and Tartaric Acids in Water, *J. Am. Chem. Soc.*, 1937, **59**, 2547–2549.
- 60 A. Apelblat, *Citric Acid*, Springer International Publishing, Cham, 2014.
- 61 G. Socrates, *Infrared and Raman Characteristic Group Frequencies: Tables and Charts*, Wiley, 3rd edn, 2004.
- 62 C. Chung, M. Lee and E. Choe, Characterization of cotton fabric scouring by FT-IR ATR spectroscopy, *Carbohydr. Polym.*, 2004, **58**, 417–420.
- 63 H. Dave, L. Ledwani, N. Chandwani, N. Chauhan and S. K. Nema, The removal of impurities from gray cotton fabric by atmospheric pressure plasma treatment and its characterization using ATR-FTIR spectroscopy, *J. Text. Inst.*, 2014, **105**, 586–596.
- 64 Z. Cai, B. Ji, K. Yan and Q. Zhu, Investigation on Reaction Sequence and Group Site of Citric Acid with Cellulose Characterized by FTIR in Combination with Two-Dimensional Correlation Spectroscopy, *Polymers*, 2019, **11**, 2071.
- 65 E. Lam and U. D. Hemraz, Preparation and Surface Functionalization of Carboxylated Cellulose Nanocrystals, *Nanomaterials*, 2021, **11**, 1641.
- 66 M. M. de Souza Lima and R. Borsali, Rodlike Cellulose Microcrystals: Structure, Properties, and Applications, *Macromol. Rapid Commun.*, 2004, **25**, 771–787.
- 67 L. Zhai, H. C. Kim, J. W. Kim and J. Kim, Simple centrifugal fractionation to reduce the size distribution of cellulose nanofibers, *Sci. Rep.*, 2020, **10**, 11744.
- 68 L. E. Díaz, L. Frydman, A. C. Olivieri and B. Frydman, Solid State NMR of Drugs: Soluble Aspirin, *Anal. Lett.*, 1987, **20**, 1657–1666.
- 69 Y. Zhou, T. Saito, L. Bergström and A. Isogai, Acid-Free Preparation of Cellulose Nanocrystals by TEMPO Oxidation and Subsequent Cavitation, *Biomacromolecules*, 2018, **19**, 633–639.
- 70 E. J. Foster, R. J. Moon, U. P. Agarwal, *et al.*, Current characterization methods for cellulose nanomaterials, *Chem. Soc. Rev.*, 2018, **47**, 2609–2679.
- 71 T. Abitbol, D. Kam, Y. Levi-Kalisman, D. G. Gray and O. Shoseyov, Surface Charge Influence on the Phase Separation and Viscosity of Cellulose Nanocrystals, *Langmuir*, 2018, **34**, 3925–3933.
- 72 A. J. Francis, C. J. Dodge and J. B. Gillow, Biodegradation of metal citrate complexes and implications for toxic-metal mobility, *Nature*, 1992, **356**, 140–142.
- 73 M. Wada, J. Sugiyama and T. Okano, Native celluloses on the basis of two crystalline phase ($I\alpha/I\beta$) system, *J. Appl. Polym. Sci.*, 1993, **49**, 1491–1496.
- 74 S. Nam, A. D. French, B. D. Condon and M. Concha, Segal crystallinity index revisited by the simulation of X-ray diffraction patterns of cotton cellulose $I\beta$ and cellulose II, *Carbohydr. Polym.*, 2016, **135**, 1–9.
- 75 A. C. W. Leung, S. Hrapovic, E. Lam, *et al.*, Characteristics and Properties of Carboxylated Cellulose Nanocrystals Prepared from a Novel One-Step Procedure, *Small*, 2011, **7**, 302–305.
- 76 A. Palme, A. Idström, L. Nordstierna and H. Brelid, Chemical and ultrastructural changes in cotton cellulose induced by laundering and textile use, *Cellulose*, 2014, **21**, 4681–4691.
- 77 S. Elazzouzi-Hafraoui, Y. Nishiyama, J.-L. Putaux, L. Heux, F. Dubreuil and C. Rochas, The Shape and Size Distribution of Crystalline Nanoparticles Prepared by Acid Hydrolysis of Native Cellulose, *Biomacromolecules*, 2008, **9**, 57–65.
- 78 H.-L. Chen and A. Yokochi, X-ray diffractometric study of microcrystallite size of naturally colored cottons, *J. Appl. Polym. Sci.*, 2000, **76**, 1466–1471.
- 79 M. S. Reid, M. Villalobos and E. D. Cranston, *Benchmarking Cellulose Nanocrystals: from the Laboratory to Industrial Production*, Langmuir, 2017, pp. 1583–1598.
- 80 C. Li, J. Evans, N. Wang, T. Guo and S. He, pH dependence of the chirality of nematic cellulose nanocrystals, *Sci. Rep.*, 2019, **9**, 11290.
- 81 E. G. Facchine, L. Bai, O. J. Rojas and S. A. Khan, Associative structures formed from cellulose nanofibrils and nanochitins are pH-responsive and exhibit tunable rheology, *J. Colloid Interface Sci.*, 2021, **588**, 232–241.
- 82 S. Spinella, A. Maiorana, Q. Qian, *et al.*, Concurrent Cellulose Hydrolysis and Esterification to Prepare a Surface-Modified Cellulose Nanocrystal Decorated with Carboxylic Acid Moieties, *ACS Sustainable Chem. Eng.*, 2016, **4**, 1538–1550.



- 83 M. Roman and W. T. Winter, *Effect of Sulfate Groups from Sulfuric Acid Hydrolysis on the Thermal Degradation Behavior of Bacterial Cellulose*, 2004.
- 84 J. Alongi and G. Malucelli, Thermal Degradation of Cellulose and Cellulosic Substrates, in *Reactions and Mechanisms in Thermal Analysis of Advanced Materials*, John Wiley & Sons, Inc., Hoboken, NJ, USA, 2015, pp. 301–332.
- 85 S. Matsuoka, H. Kawamoto and S. Saka, What is active cellulose in pyrolysis? An approach based on reactivity of cellulose reducing end, *J. Anal. Appl. Pyrolysis*, 2014, **106**, 138–146.
- 86 P. R. Sharma and A. J. Varma, Thermal stability of cellulose and their nanoparticles: Effect of incremental increases in carboxyl and aldehyde groups, *Carbohydr. Polym.*, 2014, **114**, 339–343.
- 87 O. M. Vanderfleet, M. S. Reid, J. Bras, *et al.*, Insight into thermal stability of cellulose nanocrystals from new hydrolysis methods with acid blends, *Cellulose*, 2019, **26**, 507–528.
- 88 O. M. Vanderfleet, F. D'Acierno, A. Isogai, M. J. MacLachlan, C. A. Michal and E. D. Cranston, Effects of Surface Chemistry and Counterion Selection on the Thermal Behavior of Carboxylated Cellulose Nanocrystals, *Chem. Mater.*, 2022, **34**, 8248–8261.
- 89 A. Isogai, T. Saito and H. Fukuzumi, TEMPO-oxidized cellulose nanofibers, *Nanoscale*, 2011, **3**, 71–85.
- 90 G. Chauve and J. Bras, *Industrial Point of View of Nanocellulose Materials and Their Possible Applications*, 2014, pp. 233–252.
- 91 S. W. Felman, C. Patel, B. H. Patwardhan and D. J. Solow, Recovery of citric acid from impure process streams by addition of strong acids and salts thereof, *US Pat.*, US5712131, 1998.
- 92 S. W. Felman, C. Patel, B. H. Patwardhan and D. J. Solow, Process for producing citric acid from an impure process stream, *US Pat.*, US5827700, 1998.
- 93 M. Pazouki and T. Panda, Recovery of citric acid – a review, *Bioprocess Eng.*, 1998, **19**, 435–439.
- 94 A. M. Baniel and D. Gonen, Extraction of citric acid from fermentation broth, *US Pat.*, US4994609, 1991.

